



ORIGINAL ARTICLE



Acellular pericardium: A naturally hierarchical, osteoconductive, and osteoinductive biomaterial for guided bone regeneration

Pengyue You¹ | Yuhua Liu¹ | Xinzhi Wang¹ | Bowen Li¹ | Weiyi Wu² | Lin Tang¹

¹Department of Prosthodontics, Peking University School and Hospital of Stomatology, National Clinical Research Center for Oral Diseases, National Engineering Laboratory for Digital and Material Technology of Stomatology, Beijing Key Laboratory of Digital Stomatology, No.22 Zhongguancun South Avenue, Haidian District, Beijing, 100081, P.R. China

²Department of Second Clinical Division, Peking University School and Hospital of Stomatology, National Clinical Research Center for Oral Diseases, National Engineering Laboratory for Digital and Material Technology of Stomatology, Beijing Key Laboratory of Digital Stomatology, No.22 Zhongguancun South Avenue, Haidian District, Beijing, 100081, P.R. China

Correspondence

Yuhua Liu, Department of Prosthodontics, Peking University School and Hospital of Stomatology, National Clinical Research Center for Oral Diseases, National Engineering Laboratory for Digital and Material Technology of Stomatology, Beijing Key Laboratory of Digital Stomatology, No.22 Zhongguancun South Avenue, Haidian District, Beijing, 100081, P.R. China.
Email: liuyuhua@bjmu.edu.cn

Abstract

There is great demand for an improved barrier membrane with osteogenic potential for guided bone regeneration (GBR). Natural acellular porcine pericardium (APP) is increasingly used in regenerative medicine as a kind of common extracellular matrix materials. This study aimed to investigate its potential application in GBR, especially its osteoconductive and osteoinductive properties. Bio-Gide (BG), a commercial collagen membrane, was set as the control group. APP samples were characterized by physicochemical analyses and their biological effects on human bone mesenchymal stem cells (hBMSCs) and human gingival fibroblasts (hGFs) were also examined. Additionally, the osteogenic potential of APP was tested on a bilateral critical-sized calvarial defect model. We discovered that the smooth surface of APP tended to recruit more hBMSCs. Moreover, promoted proliferation and osteogenic differentiation of hBMSCs was detected on this side of APP, with increased alkaline phosphatase activity and upregulated expression of bone-specific genes. Besides, the rough side of APP showed good biocompatibility and barrier function with hGFs. Histologic observation and analysis of calvarial defect healing over 4 weeks revealed enhanced bone regeneration under APP compared with BG and the control group. The results of this study indicate that APP is a potential osteoconductive and osteoinductive biomaterial for GBR.

KEYWORDS

bone regeneration, collagen, extracellular matrix, pericardium

1 | INTRODUCTION

Guided bone regeneration (GBR) is the most widely used clinical technique for periodontal or peri-implant bone augmentation. Its working principle is that the application of a barrier membrane can exclude nonosteogenic tissues from migrating into the defect, thereby enabling osteoprogenitors to repopulate the defect area exclusively (Omar, Elgali, Dahlin, & Thomsen, 2019; Retzepi & Donos, 2010). The set of properties for an ideal barrier membrane include biocompatibility, occlusive property, space maintenance capacity, ability to

integrate with the surrounding tissues, and manageability (Elgali, Omar, Dahlin, & Thomsen, 2017; Retzepi & Donos, 2010). To date, resorbable membranes, especially those made from natural collagen, have attracted more attention in clinical practice for their lower risk of complications such as membrane exposure or infection (Dimitriou, Mataliotakis, Calori, & Giannoudis, 2012). Membranes composed of mostly type I and III collagen possess several excellent properties such as good tissue integration, hemostasis, and rapid vascularization (Dimitriou et al., 2012). Two techniques are typically used to fabricate collagen membranes (Parenteau-Bareil, Gauvin, & Berthod, 2010). The

first involves the extraction, purification, and polymerization of native collagen to form a functional biomaterial (Parenteau-Bareil et al., 2010), such as the commercial Bio-Gide (BG). The other technique involves decellularizing tissues such as bovine or porcine small intestinal submucosa, pericardium, and dermis; these are called extracellular matrix (ECM) membranes (Parenteau-Bareil et al., 2010). Natural ECM membranes have a three-dimensional (3D) porous macrostructure and contain preserved bioactive components, including glycosaminoglycans (GAGs), glycoproteins (GPs), and abundant growth factors (Caridade & Mano, 2017). Cell-free ECMs play a key role in regenerative medicine because they can recruit stem or progenitor cells and modulate their differentiation due to their topography, in particular their microscale features and functional components (Badylak, Freytes, & Gilbert, 2009; Brown & Badylak, 2014; Caridade & Mano, 2017; Yin, Zhang, Zhang, & Jiang, 2019).

ECM membranes originating from different tissues have distinct characteristics that relate to their function. Acellular porcine pericardium (APP), a widely used ECM membrane, is used as a patch for the repair of soft tissue, such as breast, cardiovascular, arterial, and dura mater (Caballero, Sulejmani, Martin, Pham, & Sun, 2017; Gauvin et al., 2013; Mallis, Michalopoulos, Dimitriou, Kostomitsopoulos, & Stavropoulos-Giokas, 2017; Shahabipour, Banach, Johnston, Pirro, & Sahebkar, 2017). In addition to serving as a passive patch, APP regulates the behavior of cells related to soft tissue regeneration (Akbay & Onur, 2019). Recent *in vitro* studies have revealed good biocompatibility of APP with human gingival fibroblasts (hGFs) and osteoblasts (Daniel Rothamel, Fienitz, & Smeets, 2012; Talebi Ardakani, Hajizadeh, & Yadegari, 2018). Several researchers have used APP as a barrier membrane *in vivo* and have reported excellent capacity of the barrier toward soft tissues (Daniel Rothamel et al., 2012; Hwang, Kim, Kim, & Lee, 2016). Nevertheless, the effects of APP on bone regeneration, that is, osteoinductivity, require further investigation.

The objective of our study was to identify the essential physical and chemical properties of APP and to systematically evaluate its effects on osteogenesis-related cells *in vitro*. Additionally, a critical-sized calvarial defect mouse model was developed to evaluate the functions of APP on early bone regeneration *in vivo*.

2 | MATERIALS AND METHODS

2.1 | Morphology

The microstructures of two types of commercial membranes were studied using an environmental scanning electron microscope (ESEM; Quanta 200F; FEI): BonanGen APP (Bonanga Technology, China) and a BG type I collagen membrane (BG; Geistlich Pharmaceutical, Switzerland). Small pieces ($5 \times 5 \text{ mm}^2$) of dry samples were examined in the ESEM.

2.2 | Mechanical tests

Both dry and wet (soaked in phosphate-buffered saline [PBS] for 5 min) APP specimens were prepared; they had a dumbbell shape with

a 1.5-mm-wide neck. Uniaxial tensile strength testing was conducted using a universal testing machine (Universal Test Machine; Mecmesin, UK). Repeated loading and unloading was performed four times at room temperature and a crosshead speed of 10.0 mm/min.

2.3 | Biodegradation properties

The biodegradation properties of the APP and BG membranes were compared as follows. Specimens ($10 \times 10 \text{ mm}^2$) were immersed in a 12.5 U/ml collagenase solution (Sigma-Aldrich) buffered with Tris-HCl buffer (50 mM, pH 7.4) containing 5 mM of CaCl_2 at 37°C. After incubating for 1, 6, and 9 hr, specimens were carefully removed, rinsed three times with distilled water, and vacuum freeze-dried at -80°C for 3 hr. The surfaces of all dried digested specimens were observed using the ESEM.

2.4 | Cell isolate and culture

Human bone mesenchymal stem cells (hBMSCs) were isolated from the alveolar crest of two healthy males (aged 24 and 26 years) using a previously described method (Wang, Li, Guo, & Guo, 2015). hGFs were harvested from the excised gingiva of a 24-year-old female who underwent an aesthetic crown lengthening surgery using a previously reported method (Alanazi et al., 2014). All volunteers provided written consent after being fully informed of the study protocol, which adhered to the ethical principles and requirements of the Ethics Committee Board of Peking University Hospital of Stomatology.

hBMSCs were cultured in α -MEM medium (Hyclone) supplemented with 10% fetal bovine serum (FBS) (Gibco) and 2% penicillin-streptomycin (Gibco). For the osteogenic induction medium, the above medium was supplemented with 100 nM dexamethasone, 50 $\mu\text{g}/\text{ml}$ ascorbic acid, and 10 mM β -glycerophosphate. hGFs were cultured in Dulbecco's modified Eagle's medium (Invitrogen).

2.5 | hBMSC recruitment, adhesion, proliferation, and morphology

The BG membrane was the control. The APP and BG membranes were cut into pieces 5 mm in diameter. To evaluate the effects of the APP membrane on hBMSC recruitment, cells were implanted on a 96-well plate to achieve a confluence of 90–100%. The next day, both the smooth and rough sides of the membrane were placed on hBMSCs and cocultured for 7 days, then fixed in 4% paraformaldehyde in PBS for 15 min and stained with 4',6-diamidino-2-phenylindole (DAPI; Solarbio, China) at room temperature. Confocal laser scanning microscopy (CLSM; Leica, Germany) was used to observe cell recruitment. The results of this microscopy study were used to select the optimal surface for hBMSCs. For the adhesion test, approximately 5×10^3 cells were seeded on the BG and APP membranes after pretreatment in medium in a 96-well plate. At 1, 2, 3, 4,

and 24 hr, cells were twice washed gently with PBS and quantified using a cell counting kit (CCK8; Donjindo, Japan). A cell number standard curve was used to calculate the cell adhesion number. The cell adhesion rate was defined as the number of adhered cells at an indicated time divided by the number at 24 hr. About 2.5×10^3 cells were seeded for the proliferation test. The absorbance was measured using CCK8 assay at 1, 3, 5, 7, 9, 11, and 13 days. The medium was changed every 2 days.

The morphology of cell attachment and the pattern of cell proliferation were observed for approximately 5×10^3 cells seeded on BG or APP membranes in a 96-well plate. At indicated times (1 and 7 days), the membranes were fixed as described above. After washing with PBS, 5% bovine serum albumin (BSA)/PBS was added to block the unspecific staining. Next, the samples were cocultured with FITC-Phalloidin (Solarbio) and the nuclei were labeled with DAPI. Early cell adhesion and growth patterns on the different membranes were observed using CLSM.

2.6 | hGFs adhesion, proliferation, and barrier function

Cells were seeded using the method outlined above for hGFs adhesion and proliferation. For the barrier function assay, APP membranes were cut into pieces 10 mm in diameter. After pretreatment in medium in a 48-well plate, sterile plastic rings cut from the tops of 1.5-ml centrifuge tubes were placed on the specimens to prevent movement and to seal the margin of the membranes to the bottom of the plate. About 5×10^3 cells were seeded. After 3 and 7 days, the cells were stained with Phalloidin and DAPI, and then observed using CLSM.

2.7 | Osteogenic differentiation of hBMSCs

About 1×10^4 cells were seeded on APP or BG membranes in a 96-well plate for alkaline phosphatase (ALP) staining. For ALP activity quantitation, about 2.5×10^4 cells were seeded in a 48-well plate. Cells were cultured in standard osteogenic induction medium for 7 and 14 days. Staining was performed as reported previously. Briefly, cells were washed with PBS and fixed in 4% paraformaldehyde in PBS for 15 min. After another washing with PBS, cells were incubated with ALP staining solution (Cwbiotech, China) at 37°C in the dark. The ALP activity of the hBMSCs was investigated using an ALP assay kit (Nanjing Jiancheng Bioengineering Institute, China). After the prescribed period of incubation, cells were lysed with 40 μ l of 0.1% Triton X-100 solution for 15 min. The cell lysates were then centrifuged at 12,000 rpm for 30 min. The total protein amounts were detected by BCA assay (Cwbiotech). Next, 30 μ l of *p*-nitrophenyl phosphate disodium was added to the same volume of supernatant and incubated for 30 min at 37°C. The reaction was stopped by the addition of 150 μ l of NaOH solution. Finally, the mixture was read at 520 nm

using an absorbance microplate reader. The measurements were normalized by the total protein amounts.

To evaluate the expression of genes related to osteogenic differentiation, about 6×10^4 hBMSCs were seeded on APP or BG membranes in a 12-well plate and treated with osteogenic induction medium for 7 and 14 days. The level of mRNA expression was tested by real-time quantitative polymerase chain reaction (qPCR) using the SYBR Green master mix (Roche, Switzerland). In brief, total RNA was extracted using Trizol reagent (Invitrogen) following the supplier's instructions. RNA was purified and measured by the microplate reader and reverse transcription (RT) was conducted using the PrimeScript RT reagent kit (Takara, Japan). The cycle threshold values were used to calculate the relative gene expression levels by the $2^{-\Delta\Delta C_t}$ method. β -actin was used as an endogenous control. Table 1 lists the sequence of target PCR primers.

To confirm the RT-PCR results and investigate the probable signaling pathway participating in the osteogenic differentiation of hBMSCs cultured on membranes, the protein level of pSMAD 1/5 was determined using immunofluorescence (IF) staining. After fixing and thorough washing with PBS, 0.25% of Triton X-100 solution was applied to permeabilize the cells. After blocking the unspecific staining with 3% goat serum, cells were incubated with primary antibody (1:400, Cell Signaling Technology, China) in 1% BSA/PBS at 4°C overnight. Next, the cells were treated with secondary antibody (1:200, ZSGB-BIO, China) labeled by FITC 488. Finally, the cells were stained with DAPI and the membranes were observed by CLSM.

TABLE 1 Primer sequences for real-time qPCR

Gene	Primers (F = forward, R = reverse)
ALP	F: CTATCCTGGCTCCGTG R: GCTGGCAGTGGTCAGA
BSP	F: CAGGCCACGATATTATCTTTACA R: CTCCTCTTCTTCTCCTCCTC
OCN	F: GTGCAGAGTCCAGCAAAGGT R: TCAGCCAACCTGCACAGTC
OPN	F: ATGATGGCCGAGGTGATAGT R: ACCATTCAACTCCTCGCTTT
RUNX-2	F: TGGTACTGTCATGGCGGGTA R: CCATTCCTACTAGGACTCCCA
BMP-2	F: TGACGAGGTCCTGAGCGAGTTC R: TGAGTGCCTGCGATACAGGTCTAG
OSX	F: CCTCCTCAGCTCACCTTCTC R: GTTGGGAGCCCAATAGAAA
SMAD1	F: AGATGTTCCAGGCGGTTGCTTAT R: AGGCATGGAACGCTTCACC
SMAD5	F: CGTTTCCAGATTCTTTCCACCAG R: GGCTCTTCATAGGCAACAGGC
β -actin	F: CCTGGCACCCAGCACAAAT R: GGGCCGGACTCGTCACTACT

Note: Synthesized by Sangon Biotech, China.

Abbreviations: ALP, alkaline phosphatase; qPCR, quantitative polymerase chain reaction.

2.8 | Implantation in a critical-sized calvarial-defect mouse model

Six-week-old Sprague–Dawley male mice weighing 300–350 g were used to set up the bilateral critical-sized calvarial defect model to observe early bone formation. The mice were properly anesthetized during the entire operation. A 1.5–2.0 cm sagittal incision was made on the scalp, and then two calvarial defects (diameter: 5 mm; thickness: 2 mm) were created symmetrically on both sides of the parietal lobe using an electric trephine drill. Mice were randomly assigned to one of three groups: defect only (negative control; the blank group), defect implanted with BG membranes (positive control; BG group, the rough side was toward the bone defect according to the instructions), and defect implanted with APP membranes (APP group, the smooth side was toward the bone defect) ($n = 4$). The incisions were closed with 5–0 silk sutures. All animals were sacrificed after 4 weeks of healing and the calvarias containing the defects were harvested to evaluate the effects of APP on early bone healing. The tissues were fixed in 10% formalin for 24 hr, and then immersed in 10% neutral ethylenediaminetetraacetic acid solution to decalcify. The tissues were then gradually dehydrated, embedded in paraffin, and sectioned into 5- μ m-thick slices. Finally, the slices were stained with hematoxylin and eosin (H&E) and Masson's trichrome stains under standard protocols for histological observation. The area of new bone was exhibited as bone formation ratio (defined as the area of new bone divided by the defect area) and measured by Image J. All experimental procedures were conducted with permission from the Animal Research Committee of Peking University Health Science Center.

2.9 | Statistical analysis

All data are presented as the mean \pm SD. Statistical analyses were performed using SPSS software. Statistical significance was determined using the t test for independent samples and by one-way analysis of variance. A $p < .05$ was considered statistically significant.

3 | RESULTS

3.1 | Morphology

The ESEM images in Figure 1 show the distinct differences between the macro- and microstructures of APP and BG. APP had a hierarchical 3D interconnected porous structure with a smooth surface and a rough surface. The smooth surface appeared as a thin corrugated layer with somewhat oriented collagen fibers (Figure 1a), while the rough surface contained collagen fibers oriented in various directions (Figure 1b). The cross-sectional image (Figure 1c) reveals smaller pores near the smooth surface and larger ones near the rough surface. The BG membrane had a typical bilayer structure with smooth and rough surfaces as well (Figure 1d–f). The collagen fibers were more densely packed and no pores were observed in the cross-sectional image.

3.2 | Mechanical tests

The average tensile strengths of dry and wet APP were 9.95 ± 3.38 MPa and 15.51 ± 1.37 MPa, respectively. The difference was significant ($p < .05$).

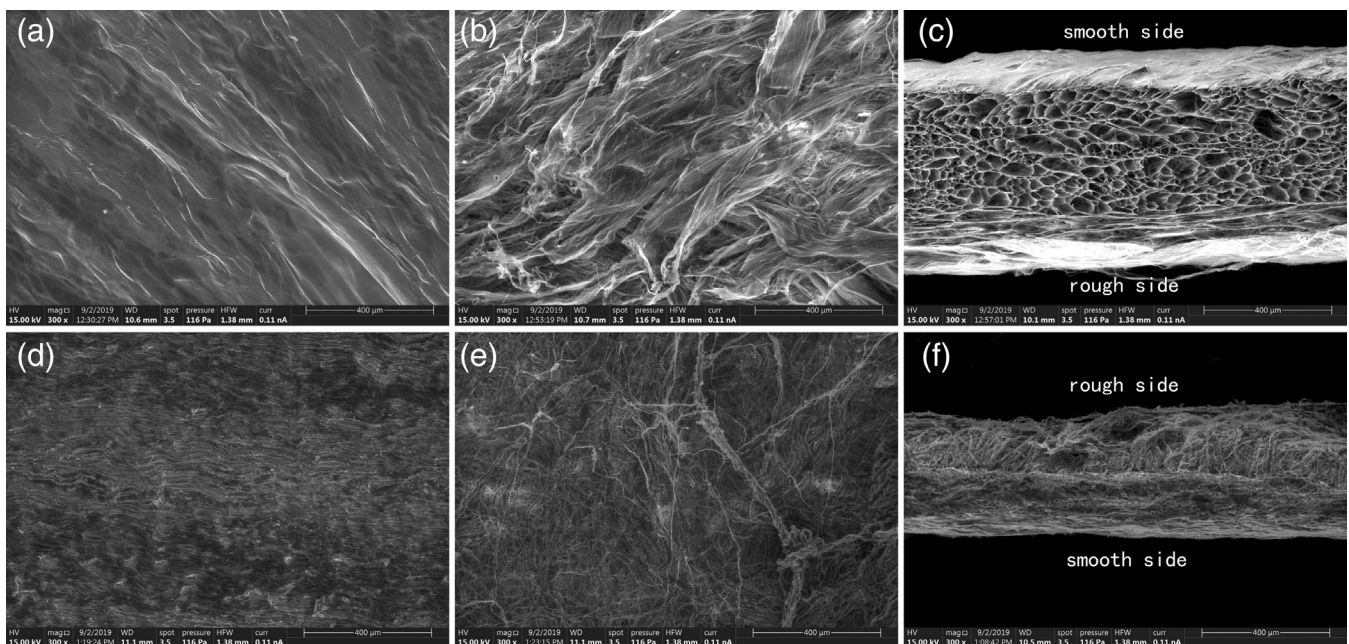


FIGURE 1 Environmental scanning electron microscope (ESEM) images of acellular porcine pericardium (APP) and Bio-Gide (BG) membrane at $\times 300$ magnification. (a) Smooth APP surface. (b) Rough APP surface. (c) Cross-sectional view of APP. (d) Smooth surface of BG. (e) Rough BG surface. (f) Cross-sectional view of BG

3.3 | Biodegradation properties

The APP microstructure was only slightly changed after 1 hr of degradation (Figure 2a,d,g) but separation of BG collagen layers occurred during this period (Figure 3a,g). After 6 hr, the thin corrugated smooth layer had degraded sufficiently to expose the underlying interconnected collagen pores (Figure 2b). The rough surface had densified (Figure 2e) and obvious pore collapse was observed (Figure 2h). For the BG membrane, the collagen layers became more separated (Figure 3h) and the collagen bundles were less compact (Figure 3b,e), especially in the smooth surface (Figure 3e). After 9 hr of degradation, the smooth side of APP had a well-aligned porous structure (Figure 2c); the rough side remained dense (Figure 2f) with depressed pores (Figure 2i), and the collagen bundles were quite loose and separated. Additionally, the smooth side seemed less enzyme-resistant than the rough side (Figure 3c,f,i).

3.4 | hBMSC recruitment, adhesion, proliferation, and morphology

Many more cells were detected on the smooth surface than on the rough surface (Figure 4). The effects of APP on the adhesion and proliferation of hBMSCs were examined. Increased adhesion was observed within 3 hr ($p < .05$), and no difference was observed after 4 hr (Figure 5a) ($p > .05$). The cells grew similarly during the first

5 days but significantly faster on APP than BG after 5 days (Figure 5b) ($p < .05$). The CLSM images clearly revealed the morphology of the hBMSCs seeded on the membranes for 1 and 7 days (Figure 5c). At Day 1, cells were well attached to both membranes and had an elongated spindle shape. Interestingly, the initial cell growth pattern was polarized on APP but random on BG. After 7 days, an oriented proliferation was more apparent on APP, while more flat cells were observed on BG. Both cell groups exhibited tight adhesion to the membrane surfaces, with filopodia and lamellipodia apparent.

3.5 | hGF adhesion, proliferation, and barrier function

The adhesion and proliferation of hGFs on APP and BG membranes did not differ significantly ($p > .05$) (Figure 6a,b). Micrographs revealed hGFs seeded on the rough side of APP (Figure 6d,e). Multilayers of cells formed at the surface and the absence of any cells within the membranes confirmed the barrier function required for GBR (Figure 6d,e).

3.6 | Osteogenic differentiation of hBMSCs

The ALP was stained and quantified to validate its effect on osteogenic differentiation of hBMSCs. ALP activity was significantly higher

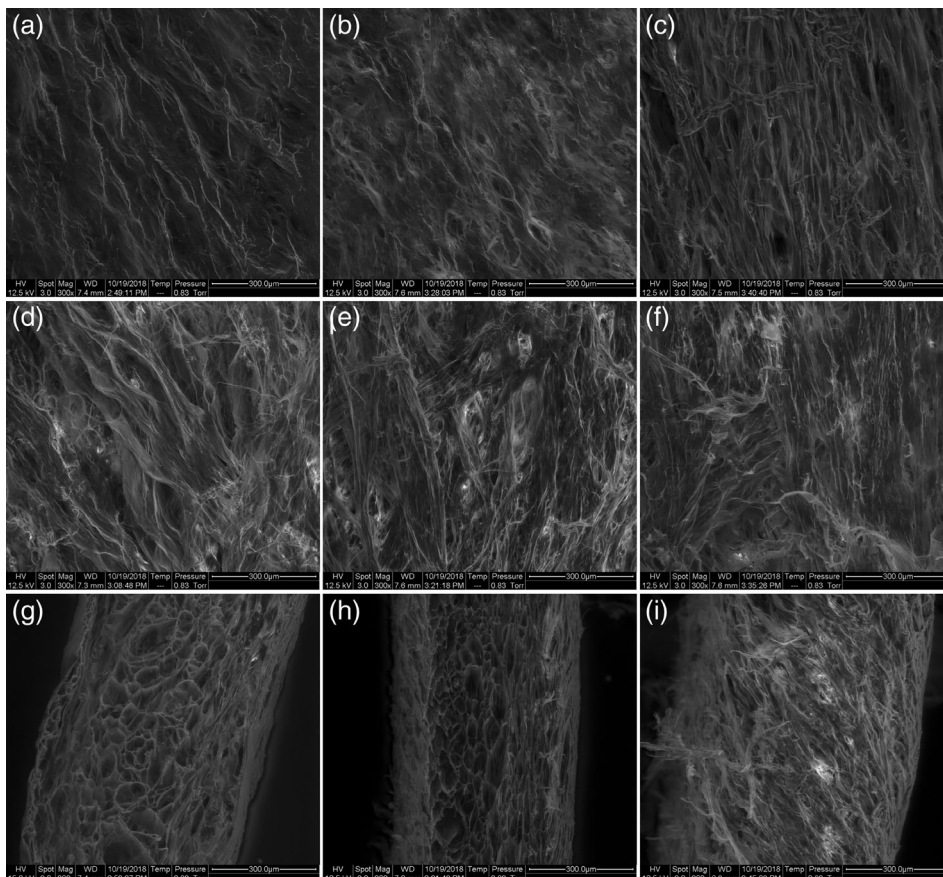


FIGURE 2 Environmental scanning electron microscope (ESEM) images of acellular porcine pericardium (APP) during enzymolysis. (a–c) Smooth surface after 1, 6, and 9 hr of degradation, respectively. (d–f) Rough surface after 1, 6, and 9 hr of degradation, respectively. (g–i) Cross-sectional images after 1, 6, and 9 hr of degradation, respectively

FIGURE 3 Environmental scanning electron microscope (ESEM) images of Bio-Gide (BG) during enzymolysis. (a–c) Smooth surface after 1, 6, and 9 hr of degradation, respectively. (d–f) Rough surface after 1, 6, and 9 hr of degradation, respectively. (g–i) Cross-sectional images after 1, 6, and 9 hr of degradation, respectively

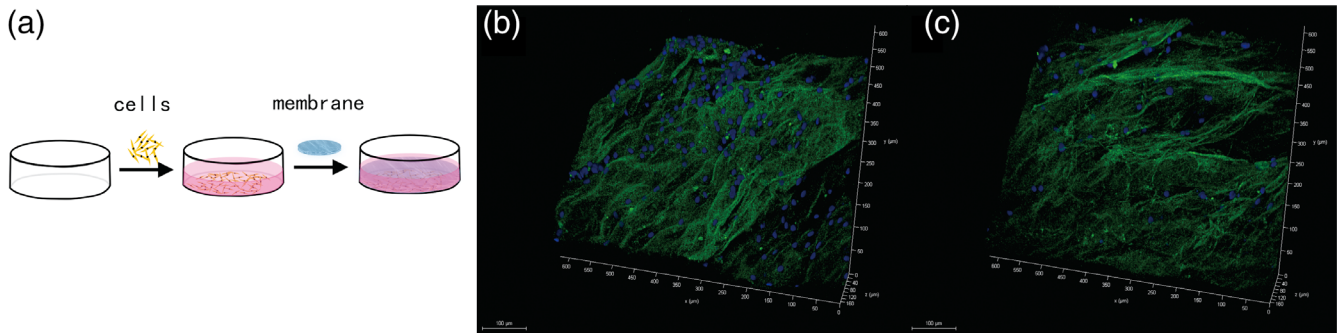
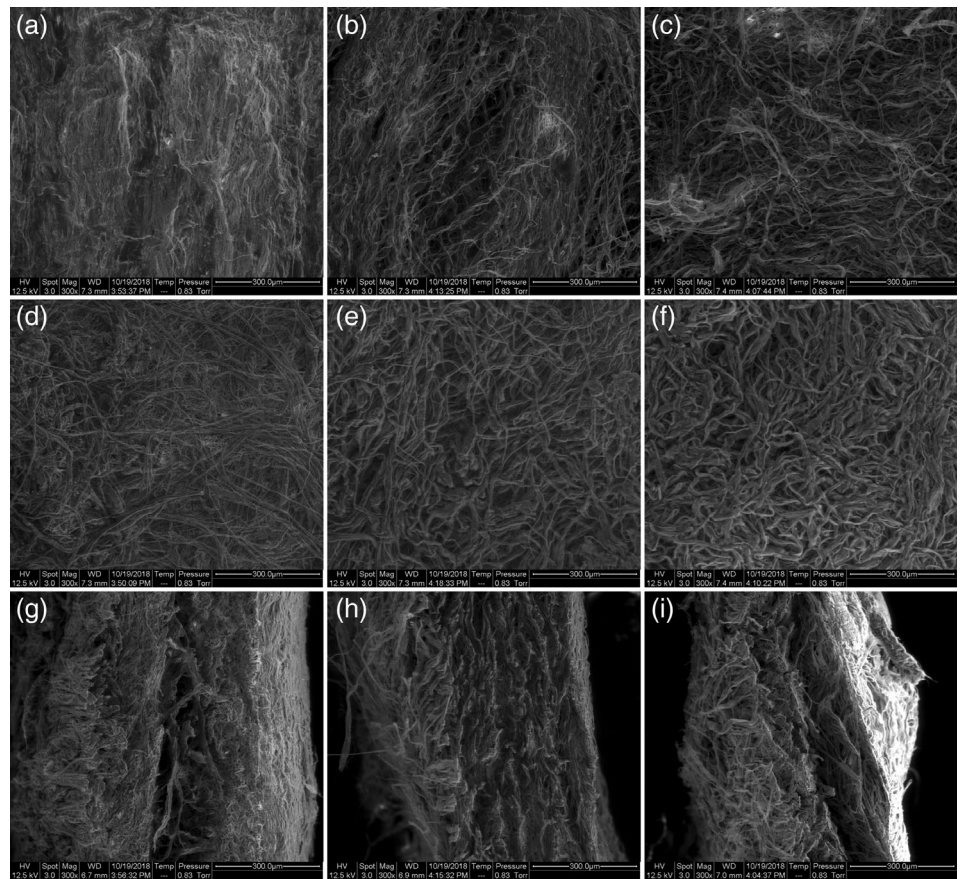


FIGURE 4 Human bone mesenchymal stem cells (hBMSCs) by the smooth and rough sides. (a) Schematic diagram of the model used to assess the effect of different acellular porcine pericardium (APP) surfaces on the recruitment of hBMSCs. (b) Cells recruited by the smooth surface. (c) Cells recruited by the rough surface. Nuclei of hBMSCs were stained blue. The collagen scaffold of APP showed green spontaneously under the laser light. More cells were recruited by the smooth side

and increased with culturing time compared with BG activity (Figure 7a) ($p < .05$). The purple spindle morphology in Figure 7b corresponds to the expression of ALP in the hBMSCs. To further evaluate the osteogenic potential, the expression of bone-specific genes was detected using RT-PCR (Figure 8). Compared with the cells on BG after 7 days, expression of all of the detected genes (ALP, BSP, OCN, OPN, RUNX-2, OSX, BMP-2, SMAD1, SMAD5) was upregulated significantly ($p < .01$), about 6.5-, 40.5-, 2.1-, 29.8-, 1.9-, 3.0-, 2.3-, 2.0-, and 2.4-fold, respectively. After 14 days, the levels of ALP, BSP, RUNX-2, BMP-2, SMAD1, and SMAD5 gene expression on APP were

upregulated with the change of about 5.7, 3.9, 1.7, 1.6, 1.9, and 1.3 times compared with Day 7, while the levels of OCN, OPN, and OSX were lower. However, significant variation remained between APP and BG in terms of the expression of OCN and OSX ($p < .01$) (about 1.2- and 2.1-fold, respectively). IF staining of pSMAD 1/5 was used to investigate whether the BMPs/SMAD signaling pathway was involved in regulating the hBMSCs differentiation (Figure 9). Although the specific triple helix of collagen and the porous structure of the membranes led to strong FITC adsorption, it was still obvious that more pSMAD 1/5 was present in the nuclei of cells cultured on APP.

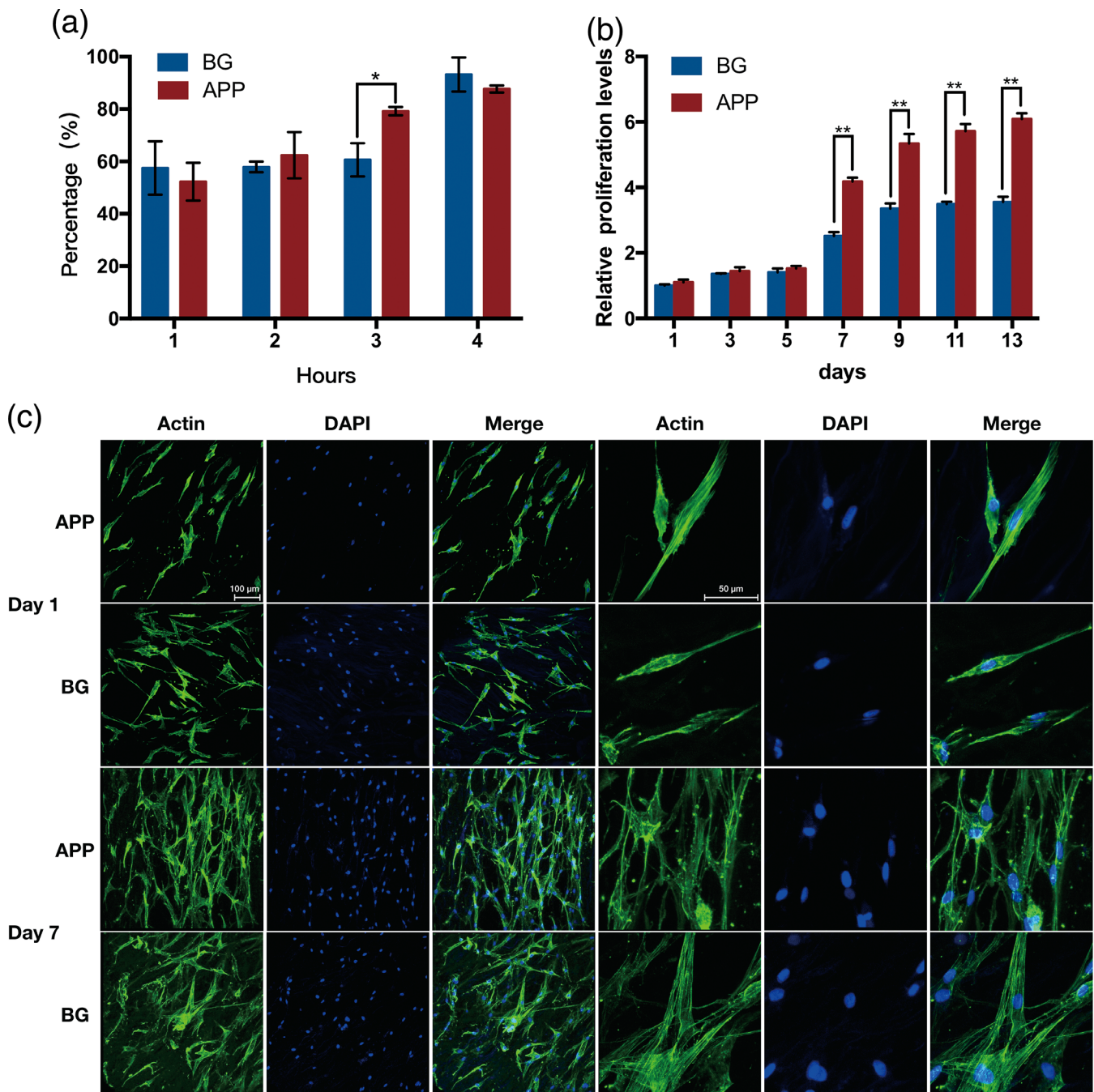


FIGURE 5 Adhesion, proliferation, and morphology of human bone mesenchymal stem cells (hBMSCs) on acellular porcine pericardium (APP) and Bio-Gide (BG) membrane. (a) The rate of cell adhesion on APP and Bio-Gide type I collagen (BG) membranes. At Hour 3, significantly more cells were adhered on APP. No distinct difference was found at Hours 1, 2, and 4. (b) Relative proliferation levels of hBMSCs implanted on APP or BG membranes for 13 days, standardized by cell number on BG at Day 1. (c) Morphology of hBMSCs seeded on APP or BG membranes for 1 and 7 days. *, $p < .05$

3.7 | Implantation in a critical-sized calvarial-defect mouse model

All animals survived the surgery and were available for evaluation. Postoperative clinical healing was uneventful in all animals. No visible complications, such as membrane exposure or infection, were observed during the entire 4-week healing period.

In the blank group, the defect was mainly occupied by a thin layer of connective tissue with many blood vessels. Little new bone was found from the original bone at the edge and the loose connective tissue above the defect was obviously thickened (Figure 10c,f). In the BG group, the defect was considerably occupied by thick provisional connective tissue. The presence of inflammatory cells indicated a mild chronic inflammation. New bone formation was, however, limited to

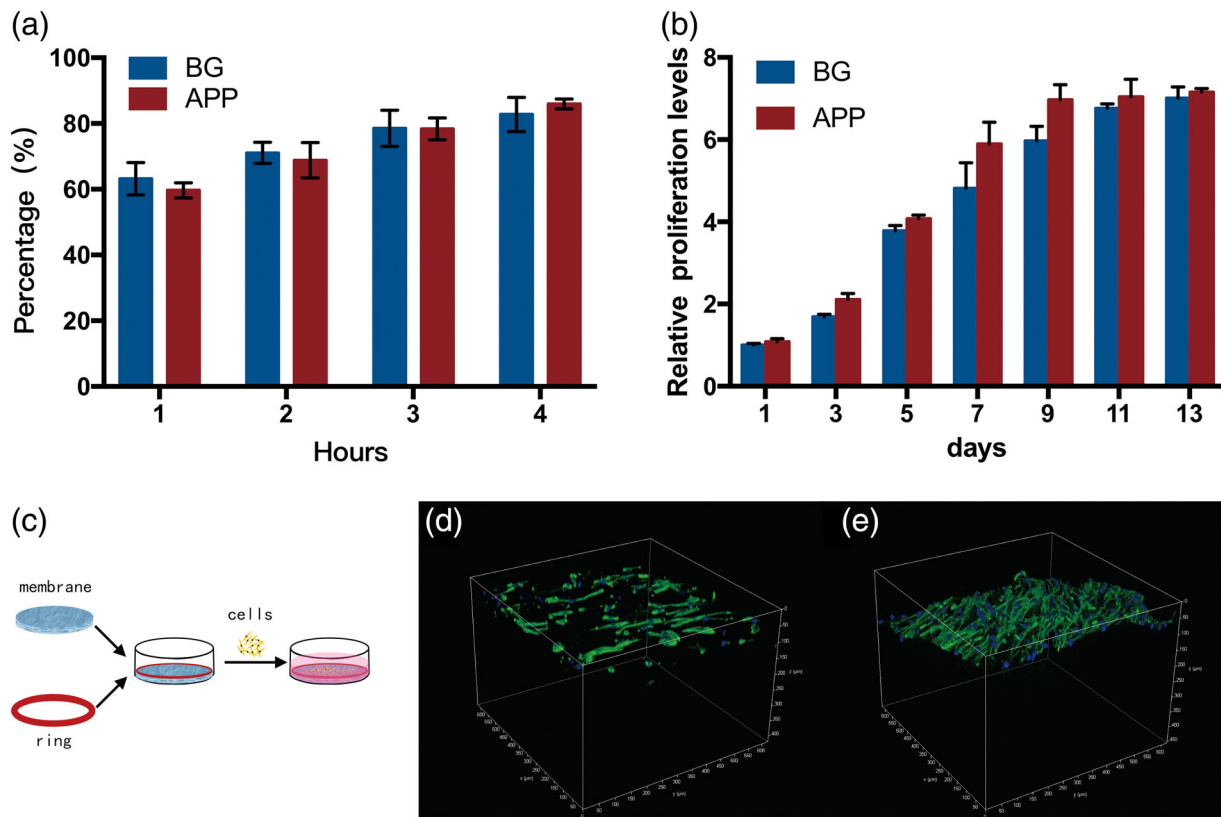


FIGURE 6 Adhesion, proliferation, and barrier function of human gingival fibroblasts (hGFs) on acellular porcine pericardium (APP) membrane. (a) The rate of cell adhesion on APP and Bio-Gide (BG) membranes. (b) Relative proliferation levels of hGFs implanted on APP or BG membranes for 13 days, standardized by cell number on BG on Day 1. (c) Schematic diagram of the model used to detect the APP barrier function. (d,e) Confocal scanning laser microscopy images of hGFs cultured on APP membranes for 3 and 7 days. *, $p < .05$

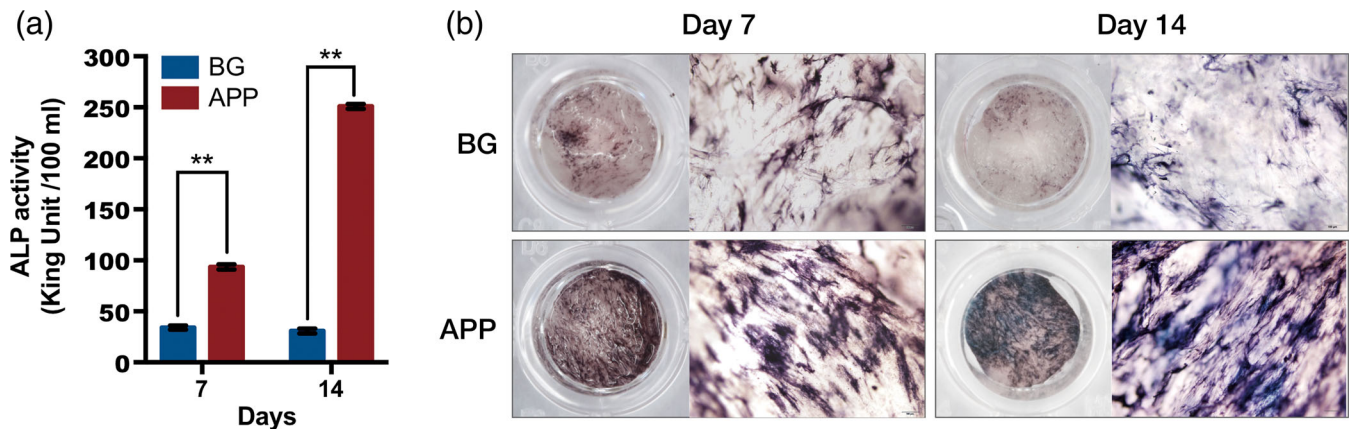


FIGURE 7 (a) Alkaline phosphatase (ALP) activity quantitation and (b) ALP staining of human bone mesenchymal stem cells (hBMSCs) after osteogenic induction for 7 and 14 days. **, $p < .01$

the defect margins (Figure 10b). The BG membrane had mostly degraded with only small fragments remaining. Almost no fibrovascular tissue was observed growing into the membrane fragments (Figure 10e). In the APP group, the defect was occupied by thick connective tissue and also new bone, which formed from the defect edge, and especially beneath the membrane. Small new bone islands and matrix were also observed near the dura mater (Figure 10a). Cubic osteoblasts were observed in close contact with the outer edge of the

newly formed bone. Similarly, infiltration of macrophages, lymphocytes, and mononuclear cells indicated mild inflammation (Figure 10d). Although degradation had thinned the APP membrane, it still presented as a complete layer and was integrated with the surrounding tissues. Abundant fibrous tissue and histocytes had grown into the membrane. Additionally, capillaries were detected in the middle of the membrane. Well-organized connective tissue with high cellularity was observed under the membrane (Figure 10d). New bone formation

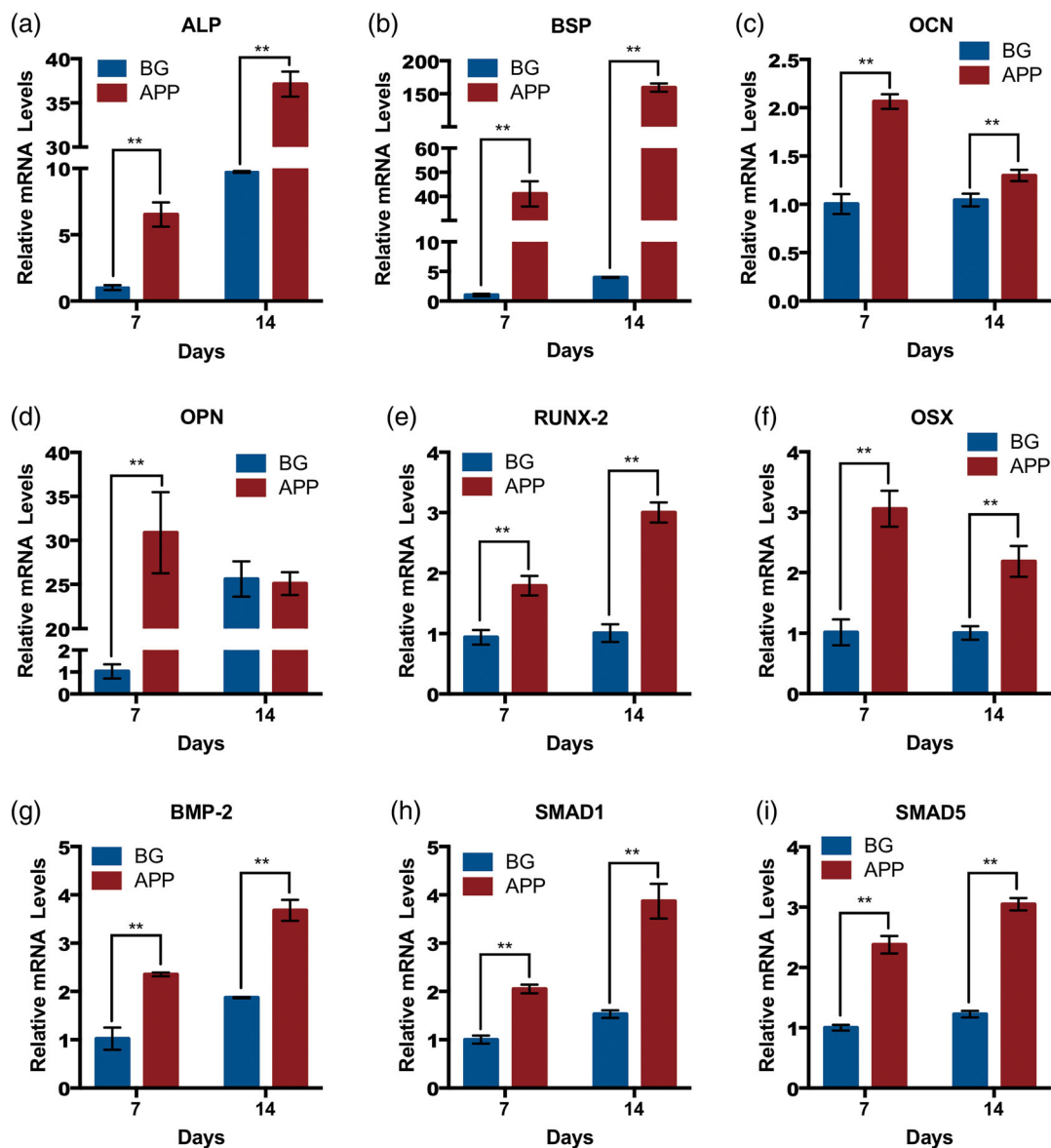


FIGURE 8 Relative mRNA levels of (a) alkaline phosphatase (ALP), (b) BSP, (c) OCN, (d) OPN, (e) RUNX-2, (f) OSX, (g) BMP-2, (h) SMAD1, and (i) SMAD5 after 7 and 14 days of osteogenic induction of human bone mesenchymal stem cells (hBMSCs) in vitro. **, $p < .01$

radio was quantified by histological analysis using H&E staining. Bone formation ratio under the APP membrane was significantly higher than the BG group and control group ($p < .05$) (Figure 11). Masson's trichrome staining was further performed to analyze the histological morphology of the newly formed tissue. Both of the APP and BG groups displayed increased collagenous matrix stained with thick blue, whereas the blank group showed mainly fibrous soft tissue stained with a little blue. The newly formed bone was mostly stained with blue for an insufficient degree of mineralization (Figure 12).

4 | DISCUSSION

Membranes for GBR should be porous, biodegradable, biocompatible, osteoconductive and osteoinductive to function effectively in

the complex osteogenic environment (Caridade & Mano, 2017). Commercial APP has already been used in reconstructive therapies, especially for soft tissue regeneration. Our in vivo data indicate that APP membranes are also beneficial for hBMSCs proliferation, osteogenic differentiation, and facilitating bone regeneration. Besides, this is the first time to report osteogenic properties of this brand of APP membrane.

An ideal barrier membrane for GBR should have a porous and hierarchical structure to enhance accessibility of bone-forming cells and prevent the invasion of undesired cells from the connective tissue (Rather, Jhala, & Vasita, 2019). We observed a porous and bilayer architecture for APP, which is consistent with previous research (Barbeck et al., 2015; Daniel Rothamel et al., 2012; Hwang et al., 2016; Tovar et al., 2019). Moreover, the collagen fibers were connected in large pores and were more oriented near the smooth side of

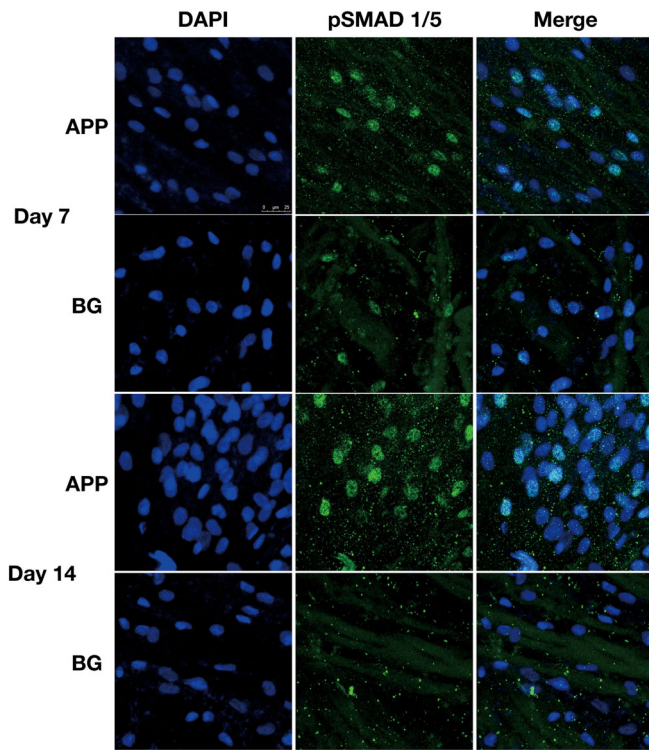


FIGURE 9 Immunofluorescence staining of pSMAD 1/5 (green) in the human bone mesenchymal stem cells (hBMSCs) cultured on acellular porcine pericardium (APP) and Bio-Gide (BG) membranes for 7 and 14 days

the membrane, while small pores and multidirectional bundles of collagen fibers were observed near the rough side (Figure 1).

The ability to maintain space is an essential characteristic for a bone regeneration membrane. Our measured tensile strength of APP was 9.95 ± 3.38 MPa when dry, which significantly increased to 15.51 ± 1.37 MPa ($p < .05$) after immersion in water for 5 min. Under the same condition of loading, Hwang et al. reported the tensile strength of dry APP of 14.15 ± 2.24 MPa and of dry BG of 6.37 ± 1.35 MPa (Hwang et al., 2016); we previously reported a tensile strength of 7.23 ± 2.05 MPa for dry BG (Wu, Li, Liu, Wang, &

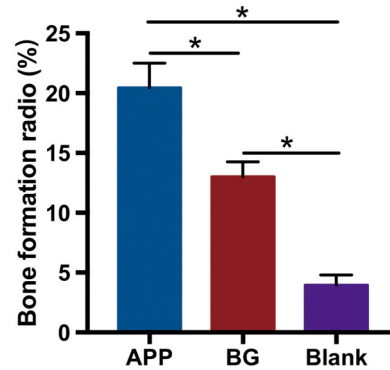


FIGURE 11 Bone formation ratio in the control defects and the defects treated with acellular porcine pericardium (APP) or Bio-Gide (BG) membranes at 4 weeks. *, $p < .05$

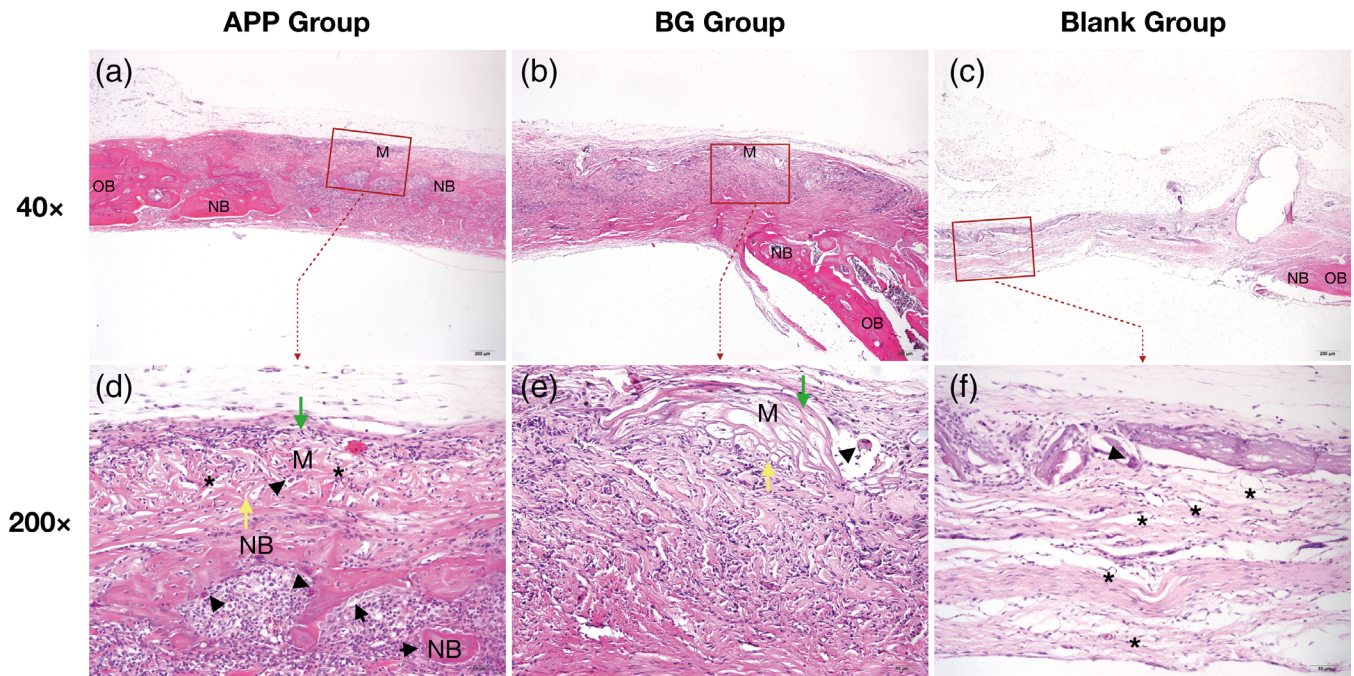


FIGURE 10 Histological transversal sections obtained at 4 weeks after surgery (hematoxylin and eosin staining). (a,d) Acellular porcine pericardium (APP) group; (b,e) Bio-Gide (BG) group; and (c,f) blank group. The boxed areas in the panels above (at $\times 40$ magnification) are magnified in the corresponding panels below. OB: original bone; NB: new bone; M: membrane; arrowhead: multinuclear giant cells; arrow: osteoblasts; asterisk: capillaries; green arrow: the surface toward soft tissue; yellow arrow: the surface toward bone defect

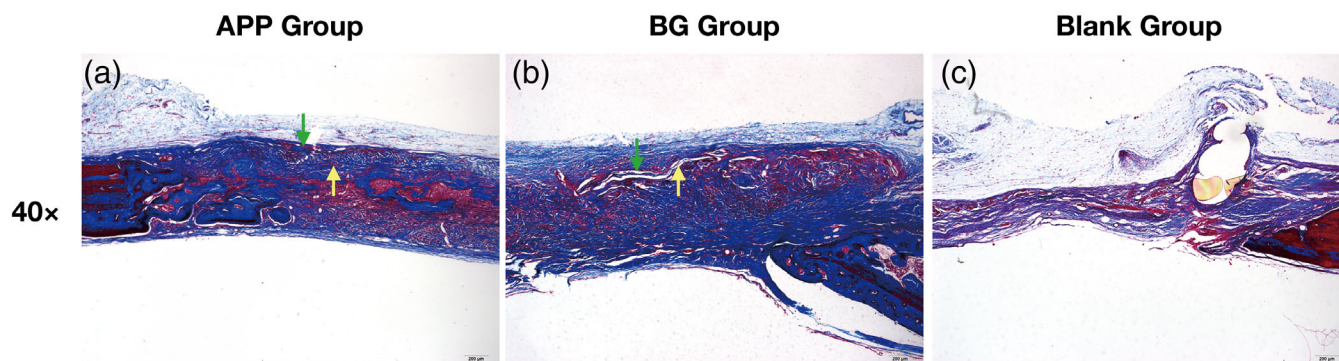


FIGURE 12 Histological transversal sections obtained at 4 weeks after surgery (Masson's trichrome staining). (a) Acellular porcine pericardium (APP) group; (b) Bio-Gide (BG) group; and (c) blank group. Green arrow: the surface toward soft tissue and yellow arrow: the surface toward bone defect. Newly formed collagenous matrix and immature bone stained as blue, and the original bone stained as red

Tang, 2018). The biomechanical properties of the pericardium are directly related with its biofunction. The collagen fibers of the pericardium are uniform and wave-like with accompanying elastic fibers (Braga-Vilela, Pimentel, Marangoni, Toyama, & de Campos Vidal, 2008; Maurer et al., 2018). Sulejmani et al. found that the smooth side of APP contributed more to its mechanical properties, and especially to its anisotropic material response (Sulejmani, Caballero, Martin, Pham, & Sun, 2019). Interestingly, Bagno et al. suggested that the collagen fiber bundles aligned in different directions in APP became more oriented with increasing applied stresses (Bagno et al., 2018). Thus, the special components, distinct microstructure, and pattern of mechanical response contributed to the better mechanical properties of APP.

Enzyme resistance capacity is another key requirement for barrier membranes (Wang et al., 2016). In the present study, ESEM was used to study changes in the membranes during enzymolysis. The microstructure of the smooth side of APP having oriented fibers and interconnected pores tended to be more stable; the rough side maintained its dense porosity during the first 6 hr of biodegradation. Additionally, a porous layer of APP was clearly evident after implantation in the mouse calvarial defect; in the BG case, only fragments of BG membrane were observed. Previous *in vivo* studies have reported an approximate 3-month biodegradation period for APP (Daniel Rothamel et al., 2012).

The effects of APP on hBMSC recruitment, adhesion, proliferation, and osteogenic differentiation were explored in detail, potential about osteoconductivity and osteoinductivity of APP could be concluded from the results. The smooth surface (the serosa) tended to attract more hBMSCs, which meant that this surface was the implantation side. Our data did not reveal any difference in hBMSC adhesion between APP and BG. However, APP facilitated hBMSC proliferation significantly and obvious polar growth of cells was observed. Additionally, the genes related to osteogenesis were significantly upregulated on APP. RUNX-2 and ALP are the most frequently used markers associated with the early phase of osteogenesis (Zolocinska, 2018). RUNX-2, regulated by BMP-2, is the most important transcription factor in osteogenesis and mediates the expression of BSP, OCN

and OPN²⁹. ALP is closely responsible for the mineralization of ECM and can alleviate the inhibition of OPN on bone mineralization (Halling Linder et al., 2017; Zolocinska, 2018). OPN, OCN and BSP are late markers of osteogenic differentiation (Zolocinska, 2018). OPN and OCN show inhibitory effects on bone mineralization, while BSP is a major structural protein of bone matrix (Kruger, Miller, Godwin, & Wang, 2014; Zoch, Clemens, & Riddle, 2016). OSX is a classical osteogenic marker and essential for the activation of bone-specific genes. BMP-2 is also highly expressed in early osteogenesis (Sinha & Zhou, 2013). BMPs/SMAD pathway is crucial for the regulation of hBMSCs differentiation (Grafe et al., 2018). Since high expression of BMP-2, SMAD1, and SMAD5 were observed, we explored the probable mechanism of APP promoting hBMSC differentiation. IF staining of pSMAD 1/5 was performed, and more expression was detected on APP. Collagen scaffolds activate the BMPs signaling pathway (Li, Zhang, Cheng, Gu, & Zhao, 2017; Rao, Harini, Shadamarsan, Balagangadharan, & Selvamurugan, 2018). BMPs phosphorylate SMAD proteins by interaction with specific receptors (Rao et al., 2018). As transcriptional complexes, SMADs act as signal transducers that bind to a specific DNA sequence in the nucleus (Rao et al., 2018). The signaling pathway activation caused apparent nuclear localization of pSMAD 1/5 (Rao et al., 2018). As the downstream gene of this pathway, the expression of RUNX-2 would be promoted (Rao et al., 2018). The findings of the present study revealed the activation and participation of the BMPs signaling pathway in hBMSC differentiation on APP *in vitro*. Other probable signaling pathways remain to be explored.

An optimal biomaterial for GBR should also possess osteoconductivity and osteoinductivity. Osteoconductivity involves the recruitment and proliferation of immature cells, while osteoinductivity means triggering the osteogenic differentiation (Bosetti et al., 2014; Kouketsu et al., 2020). Though these are two independent patterns, they are both regulated by ECM microenvironment in a complex manner, which is related to the composition, mechanical properties, surface topography, surface wettability and 3D geometrical features of ECM (Chen et al., 2018; Li, Xiao, & Liu, 2017). We observed better recruitment of hBMSCs in the smooth side than the

rough side and established promoted osteogenic differentiation of hBMSCs in this side. A layer of mesothelial cells lined the smooth surface of the porcine pericardium before decellularization (Sicari et al., 2014). We hypothesized that the curvature and diameter of collagen fibers and cell-recognizing receptors preserved after decellularization in the smooth side might contribute to recruiting hBMSCs. Besides, polar proliferation was observed in the smooth surface. Recent researches have reported that cells in an organized alignment were more likely to differentiate into an osteogenic type (Zhu, Luo, & Liu, 2020). Promoted differentiation of stem cells (such as MSCs and ADMSCs) toward osteoblasts was found on aligned nanofibers compared with the random structure (Chen, Qian, et al., 2016; Pandey, Rathore, Johnson, & Cekanova, 2018; Ren et al., 2019). These findings suggest that the orientation of collagen fibers mimicking the anisotropic structure of bone might contribute to the facilitated osteogenesis on APP compared with BG. Additionally, surface wettability, porosity and biomechanical properties could also regulate initial cell recruitment, migration, proliferation as well as differentiation (Martino, D'Angelo, Armentano, Kenny, & Orlicchio, 2012). Hence, the smooth surface of APP might be more suitable for bone formation. Recent studies have reported the effects of APP on cell behavior. Rothamel et al. demonstrated promoted proliferation of osteoblasts on APP compared with BG, consistent with our findings, but no further investigation was conducted (Daniel Rothamel et al., 2012). Mergerle et al. observed continuous production of hyaluronic acid after seeding human sheath synoviocytes and adipose-derived stem cells (hADSCs) on APP, and observed similar polar growth of hADSCs on the smooth side (Megerle et al., 2016). Because both APP and BG membranes had similar collagen I composition, the different effects on hBMSCs might be due to the special components and microstructure of the ECM. Many studies have reported functional components, such as GAGs and GPs, which can mediate the interaction between cells and the ECM (Cigliano et al., 2012; Gaffney, Wrona, & Freytes, 2017; Mallis et al., 2017). GAGs are reported to determine the interaction with BMP-2 and the formation of BMP-2/BMP receptor IA, which plays a key role in BMP related bone formation (Chen, Wang, & Liu, 2016). Fibronectin (Fn), a kind of GPs, is associated with altering BMP receptor location through binding with integrin $\alpha 1$, which is essential for BMP-triggered signal transduction (Chen, Wang, & Liu, 2016).

The findings of the mouse calvarial defect model confirmed the osteoconductive and osteoinductive capacities of APP in vivo. Healing of a calvarial defect involves intramembranous ossification, which relies on direct differentiation of mesenchymal precursor cells into osteoblasts (Runyan & Gabrick, 2017). In the present study, we observed newly formed bone on the edge of the defect in the BG group, while new bone was discovered on the edge and under the membrane in the APP group. Bone vessels and newly formed collagenous matrix were also found growing into the pores of APP. Infiltration of inflammation cell-like macrophages, lymphocytes, mononuclear cells, and multinuclear giant cells was observed in and around the APP. The presence of macrophages and multinuclear giant cells contribute to the biodegradation of biomaterials and to tissue

regeneration. Reza et al. implanted APP subcutaneously in a mouse dorsum model and found angiogenesis and M2 macrophages recruitment that were closely related to tissue regeneration (Reza Khorramirouz, Noble, Morse, Lerman, & Young, 2019). Rothamel et al. applied APP as the barrier membrane in canine ridge preservation, and found that APP facilitated early vascularization and integration with the surrounding tissues (Daniel Rothamel et al., 2012). Moreover, Mendoza-Novelo et al. found that during biodegradation, the acellular bovine pericardium released molecules such as fibronectin, laminin, and GAG, all of which are well-known factors involved in cell adhesion and growth, which activated M2 macrophages and enhanced vascularization (Mendoza-Novelo et al., 2016). The action of ECM degradation components is another potential mechanism of ECM modulating tissue regeneration (Robb, Shridhar, & Flynn, 2017). With the degradation of ECM by host cells, a wide variety of cryptic peptides termed matrikines are generated, which are known to recruit stem cells and regulate cell behaviors, angiogenesis as well as immune response (Robb et al., 2017; Sicari et al., 2014). Bone regeneration in vivo is much more complex than that in vitro because it involves interactions between cells and the environment. Deeper research is needed to explore the dynamic changes in APP during bone regeneration.

5 | CONCLUSIONS

This study demonstrated that APP is a potential osteoconductive and osteoinductive biomaterial for GBR. Compared with the commercial collagen membrane (BG), the smooth side of APP led to pronounced differences in recruitment, proliferation, and osteogenic differentiation of hBMSCs. Without infiltration, the rough side of APP also served as a good barrier for hGFs. The BMPs pathway was activated during the process of osteogenic differentiation of hBMSCs in vitro. More importantly, APP effectively enhanced in vivo bone regeneration. Our findings provide evidence for clinical applications of APP in bone tissue engineering.

CONFLICT OF INTEREST

The authors declare that there are no conflicts of interest regarding the publication of this article.

REFERENCES

- Akbay, E., & Onur, M. A. (2019). Investigation of survival and migration potential of differentiated cardiomyocytes transplanted with decellularized heart scaffold. *Journal of Biomedical Materials Research. Part A*, 107, 561–570.
- Alanazi, H., Semaili, A., Perraud, L., Chmielewski, W., Zakrzewski, A., & Rouabhia, M. (2014). Cigarette smoke-exposed *Candida albicans* increased chitin production and modulated human fibroblast cell responses. *BioMed Research International*, 2014, 963156.
- Badylak, S. F., Freytes, D. O., & Gilbert, T. W. (2009). Extracellular matrix as a biological scaffold material: Structure and function. *Acta Biomaterialia*, 5, 1–13.
- Bagno, A., Aguiari, P., Fiorese, M., Iop, L., Spina, M., & Gerosa, G. (2018). Native bovine and porcine pericardium respond to load with additive recruitment of collagen fibers. *Artificial Organs*, 42, 540–548.

- Barbeck, M., Lorenz, J., Holthaus, M. G., Raetscho, N., Kubesch, A., Booms, P., ... Ghanaati, S. (2015). Porcine dermis and pericardium-based, non-cross-linked materials induce multinucleated giant cells after their in vivo implantation: A physiological reaction? *The Journal of Oral Implantology*, 41, e267–e281.
- Bosetti, M., Fusaro, L., Nicoli, E., Borrone, A., Aprile, S., & Cannas, M. (2014). Poly-L-lactide acid-modified scaffolds for osteoinduction and osteoconduction. *Journal of Biomedical Materials Research. Part A*, 102, 3531–3539.
- Braga-Vilela, A. S., Pimentel, E. R., Marangoni, S., Toyama, M. H., & de Campos Vidal, B. (2008). Extracellular matrix of porcine pericardium: Biochemistry and collagen architecture. *The Journal of Membrane Biology*, 221, 15–25.
- Brown, B. N., & Badylak, S. F. (2014). Extracellular matrix as an inductive scaffold for functional tissue reconstruction. *Translational Research*, 163, 268–285.
- Caballero, A., Sulejmani, F., Martin, C., Pham, T., & Sun, W. (2017). Evaluation of transcatheter heart valve biomaterials: Biomechanical characterization of bovine and porcine pericardium. *Journal of the Mechanical Behavior of Biomedical Materials*, 75, 486–494.
- Caridade, S. G., & Mano, J. F. (2017). Engineering membranes for bone regeneration. *Tissue Engineering. Part A*, 23, 1502–1533.
- Chen, H., Qian, Y., Xia, Y., Chen, G., Dai, Y., Li, N., ... Gu, N. (2016). Enhanced osteogenesis of ADSCs by the synergistic effect of aligned fibers containing collagen I. *ACS Applied Materials & Interfaces*, 8, 29289–29297.
- Chen, R., Wang, J., & Liu, C. (2016). Biomaterials act as enhancers of growth factors in bone regeneration. *Advanced Functional Materials*, 26, 8810–8823.
- Chen, X., Fan, H., Deng, X., Wu, L., Yi, T., Gu, L., ... Zhang, X. (2018). Scaffold structural microenvironmental cues to guide tissue regeneration in bone tissue applications. *Nanomaterials (Basel)*, 8, 960.
- Cigliano, A., Gandaglia, A., Lepedda, A. J., Zinellu, E., Naso, F., Gastaldello, A., et al. (2012). Fine structure of glycosaminoglycans from fresh and decellularized porcine cardiac valves and pericardium. *Biochemistry Research International*, 2012, 979351.
- Daniel Rothamel, F. S., Fienitz, T., & Smeets, R. (2012). Biocompatibility and biodegradation of a native porcine pericardium membrane: Results of in vitro and in vivo examinations. *The International Journal of Oral & Maxillofacial Implants*, 27, 146–154.
- Dimitriou, R., Mataliotakis, G. I., Calori, G. M., & Giannoudis, P. V. (2012). The role of barrier membranes for guided bone regeneration and restoration of large bone defects: Current experimental and clinical evidence. *BMC Medicine*, 10, 81–105.
- Elgali, I., Omar, O., Dahlin, C., & Thomsen, P. (2017). Guided bone regeneration: Materials and biological mechanisms revisited. *European Journal of Oral Sciences*, 125, 315–337.
- Gaffney, L., Wrona, E. A., & Freytes, D. O. (2017). Potential synergistic effects of stem cells and extracellular matrix scaffolds. *ACS Biomaterials Science & Engineering*, 4, 1208–1222.
- Gauvin, R., Marinov, G., Mehri, Y., Klein, J., Li, B., Larouche, D., ... Guidoin, R. (2013). A comparative study of bovine and porcine pericardium to highlight their potential advantages to manufacture percutaneous cardiovascular implants. *Journal of Biomaterials Applications*, 28, 552–565.
- Grafe, I., Alexander, S., Peterson, J. R., Snider, T. N., Levi, B., Lee, B., & Mishina, Y. (2018). TGF-beta family signaling in mesenchymal differentiation. *Cold Spring Harbor Perspectives in Biology*, 10, a022202.
- Halling Linder, C., Ek-Rylander, B., Krumpel, M., Norgard, M., Narisawa, S., Millan, J. L., ... Magnusson, P. (2017). Bone alkaline phosphatase and tartrate-resistant acid phosphatase: Potential co-regulators of bone mineralization. *Calcified Tissue International*, 101, 92–101.
- Hwang, J. W., Kim, S., Kim, S. W., & Lee, J. H. (2016). Effect of extracellular matrix membrane on bone formation in a rabbit Tibial defect model. *BioMed Research International*, 2016, 1–8.
- Kouketsu, A., Matsui, K., Kawai, T., Ezoe, Y., Yanagisawa, T., Yasuda, A., ... Kamakura, S. (2020). Octacalcium phosphate collagen composite stimulates the expression and activity of osteogenic factors to promote bone regeneration. *Journal of Tissue Engineering and Regenerative Medicine*, 14, 99–107.
- Kruger, T. E., Miller, A. H., Godwin, A. K., & Wang, J. (2014). Bone sialoprotein and osteopontin in bone metastasis of osteotropic cancers. *Critical Reviews in Oncology/Hematology*, 89, 330–341.
- Li, M., Zhang, C., Cheng, M., Gu, Q., & Zhao, J. (2017). Small intestinal submucosa: A potential osteoconductive and osteoinductive biomaterial for bone tissue engineering. *Materials Science & Engineering. C, Materials for Biological Applications*, 75, 149–156.
- Li, Y., Xiao, Y., & Liu, C. (2017). The horizon of materiobiology: A perspective on material-guided cell behaviors and tissue engineering. *Chemical Reviews*, 117, 4376–4421.
- Mallis, P., Michalopoulos, E., Dimitriou, C., Kostomitsopoulos, N., & Stavropoulos-Giokas, C. (2017). Histological and biomechanical characterization of decellularized porcine pericardium as a potential scaffold for tissue engineering applications. *Bio-Medical Materials and Engineering*, 28, 477–488.
- Martino, S., D'Angelo, F., Armentano, I., Kenny, J. M., & Orlacchio, A. (2012). Stem cell-biomaterial interactions for regenerative medicine. *Biotechnology Advances*, 30, 338–351.
- Maurer, T., Stoffel, M. H., Belyaev, Y., Stiefel, N. G., Vidondo, B., Kuker, S., ... Balmer, J. (2018). Structural characterization of four different naturally occurring porcine collagen membranes suitable for medical applications. *PLoS One*, 13, e0205027.
- Megerle, K., Woon, C., Kraus, A., Raghavan, S., Pham, H., & Chang, J. (2016). Flexor tendon sheath engineering using decellularized porcine pericardium. *Plastic and Reconstructive Surgery*, 138, 630e–641e.
- Mendoza-Novelo, B., Castellano, L. E., Padilla-Miranda, R. G., Lona-Ramos, M. C., Cuéllar-Mata, P., Vega-González, A., ... Ávila, E. E. (2016). The component leaching from decellularized pericardial bio-scaffolds and its implication in the macrophage response. *Journal of Biomedical Materials Research. Part A*, 104, 2810–2822.
- Omar, O., Elgali, I., Dahlin, C., & Thomsen, P. (2019). Barrier membranes: More than the barrier effect? *Journal of Clinical Periodontology*, 46 (Suppl 21), 103–123.
- Pandey, S., Rathore, K., Johnson, J., & Cekanova, M. (2018). Aligned nanofiber material supports cell growth and increases osteogenesis in canine adipose-derived mesenchymal stem cells in vitro. *Journal of Biomedical Materials Research. Part A*, 106, 1780–1788.
- Parenteau-Bareil, R., Gauvin, R., & Berthod, F. (2010). Collagen-based biomaterials for tissue engineering applications. *Materials*, 3, 1863–1887.
- Rao, S. H., Harini, B., Shadamarshan, R. P. K., Balagangadharan, K., & Selvamurugan, N. (2018). Natural and synthetic polymers/bioceramics/bioactive compounds-mediated cell signalling in bone tissue engineering. *International Journal of Biological Macromolecules*, 110, 88–96.
- Rather, H. A., Jhala, D., & Vasita, R. (2019). Dual functional approaches for osteogenesis coupled angiogenesis in bone tissue engineering. *Materials Science & Engineering. C, Materials for Biological Applications*, 103, 109761.
- Ren, X., Li, J., Li, J., Jiang, Y., Li, L., Yao, Q., ... Xu, H. (2019). Aligned porous fibrous membrane with a biomimetic surface to accelerate cartilage regeneration. *Chemical Engineering Journal*, 370, 1027–1038.
- Retzepi, M., & Donos, N. (2010). Guided bone regeneration: Biological principle and therapeutic applications. *Clinical Oral Implants Research*, 21, 567–576.
- Reza Khorramirouz, J. L. G., Noble, C., Morse, D., Lerman, A., & Young, M. D. (2019). In vivo response of acellular porcine pericardial for tissue engineered transcatheter aortic valves. *Scientific Reports*, 9, 1094.
- Robb, K. P., Shridhar, A., & Flynn, L. E. (2017). Decellularized matrices as cell-instructive scaffolds to guide tissue-specific regeneration. *ACS Biomaterials Science & Engineering*, 4, 3627–3643.

- Runyan, C. M., & Gabrick, K. S. (2017). Biology of bone formation, fracture healing, and distraction osteogenesis. *The Journal of Craniofacial Surgery*, 28, 1380–1389.
- Shahabipour, F., Banach, M., Johnston, T. P., Pirro, M., & Sahebkar, A. (2017). Novel approaches toward the generation of bioscaffolds as a potential therapy in cardiovascular tissue engineering. *International Journal of Cardiology*, 228, 319–326.
- Sicari, B. M., Dziki, J. L., Siu, B. F., Medberry, C. J., Dearth, C. L., & Badylak, S. F. (2014). The promotion of a constructive macrophage phenotype by solubilized extracellular matrix. *Biomaterials*, 35(30), 8605–8612.
- Sinha, K. M., & Zhou, X. (2013). Genetic and molecular control of osterix in skeletal formation. *Journal of Cellular Biochemistry*, 114, 975–984.
- Sulejmani, F., Caballero, A., Martin, C., Pham, T., & Sun, W. (2019). Evaluation of transcatheter heart valve biomaterials: Computational modeling using bovine and porcine pericardium. *Journal of the Mechanical Behavior of Biomedical Materials*, 97, 159–170.
- Talebi Ardakani, M. R., Hajizadeh, F., & Yadegari, Z. (2018). Comparison of attachment and proliferation of human gingival fibroblasts on different collagen membranes. *Annals of Maxillofacial Surgery*, 8, 218–223.
- Tovar, N., Witek, L., Neiva, R., Marao, H. F., Gil, L. F., Atria, P., ... Coelho, P. G. (2019). In vivo evaluation of resorbable supercritical CO₂-treated collagen membranes for class III furcation-guided tissue regeneration. *Journal of Biomedical Materials Research. Part B, Applied Biomaterials*, 107, 1320–1328.
- Wang, H. X., Li, Z. Y., Guo, Z. K., & Guo, Z. K. (2015). Easily-handled method to isolate mesenchymal stem cells from coagulated human bone marrow samples. *World Journal of Stem Cells*, 7, 1137–1144.
- Wang, J., Wang, L., Zhou, Z., Lai, H., Xu, P., Liao, L., & Wei, J. (2016). Biodegradable polymer membranes applied in guided bone/tissue regeneration: A review. *Polymers (Basel)*, 8, 115.
- Wu, W., Li, B., Liu, Y., Wang, X., & Tang, L. (2018). Effect of multilaminar small intestinal submucosa as a barrier membrane on bone formation in a rabbit mandible defect model. *BioMed Research International*, 2018, 3270293.
- Yin, S., Zhang, W., Zhang, Z., & Jiang, X. (2019). Recent advances in scaffold design and material for vascularized tissue-engineered bone regeneration. *Advanced Healthcare Materials*, 8, 1801433.
- Zhu, L., Luo, D., & Liu, Y. (2020). Effect of the nano/microscale structure of biomaterial scaffolds on bone regeneration. *International Journal of Oral Science*, 12, 6.
- Zoch, M. L., Clemens, T. L., & Riddle, R. C. (2016). New insights into the biology of osteocalcin. *Bone*, 82, 42–49.
- Zolocinska, A. (2018). The expression of marker genes during the differentiation of mesenchymal stromal cells. *Advances in Clinical and Experimental Medicine*, 27, 717–723.

How to cite this article: You P, Liu Y, Wang X, Li B, Wu W, Tang L. Acellular pericardium: A naturally hierarchical, osteoconductive, and osteoinductive biomaterial for guided bone regeneration. *J Biomed Mater Res*. 2021;109:132–145. <https://doi.org/10.1002/jbm.a.37011>